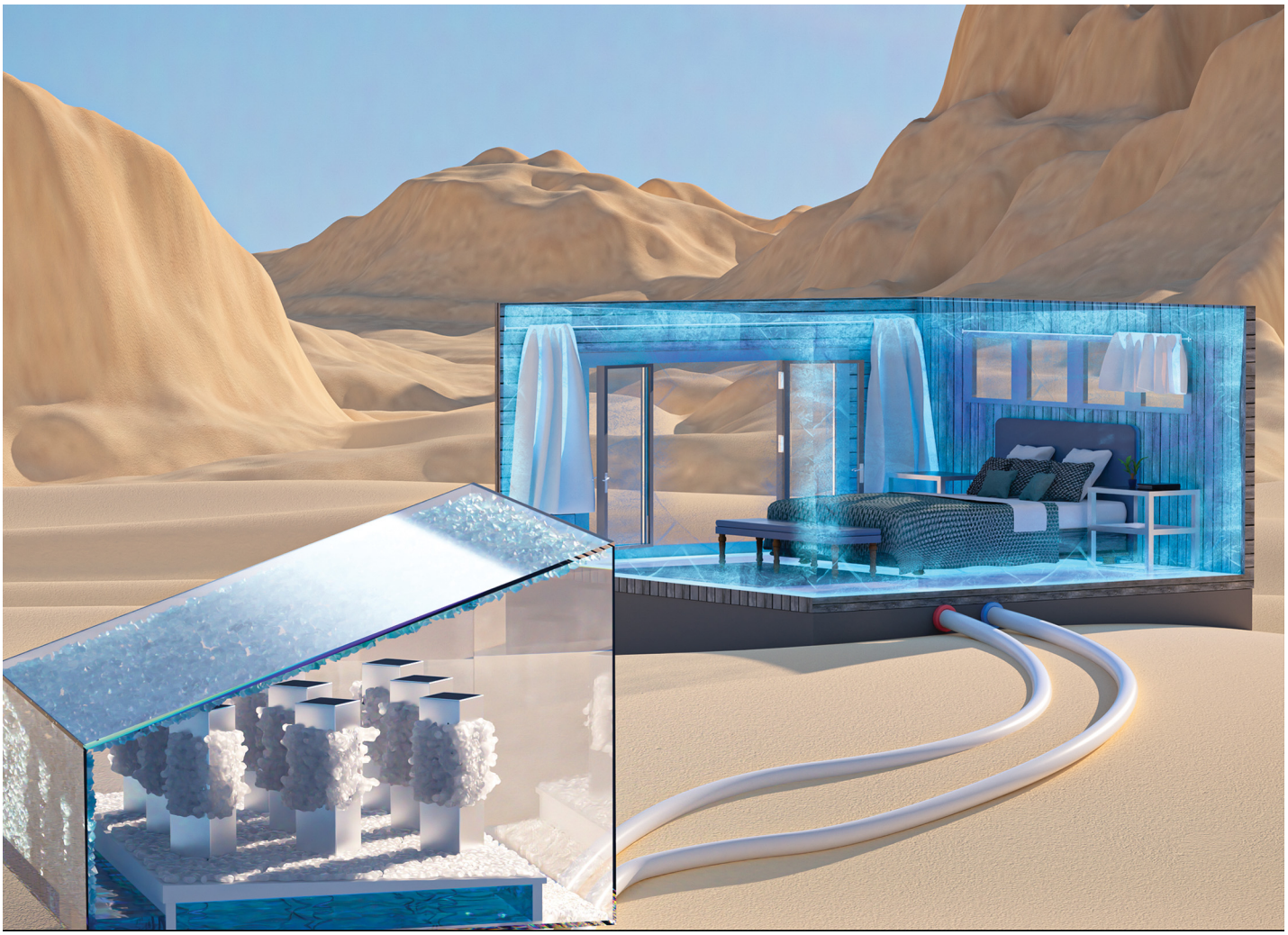

**Showcasing research from Professor Peng Wang's laboratory, Water Desalination and Reuse Center, King Abdullah University of Science and Technology, Thuwal, Saudi Arabia.**

Conversion and storage of solar energy for cooling

A simple salt-dissolution-based passive cooling system is fully driven by solar energy and offers low-cost food refrigeration and living space cooling for impoverished communities with no access to the electricity grid. The cooling power of such a system could reach up to 191 W/m$^2$. Importantly, the passive cooling design separates the dissolution cooling and solute regeneration physically and time-wise, allowing for energy storage and utilization even across seasons.

## As featured in:

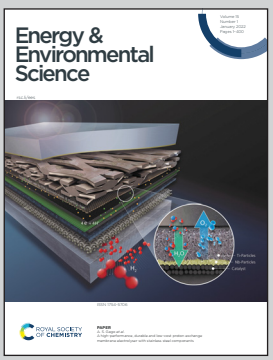


See Peng Wang *et al.*, *Energy Environ. Sci.*, 2022, **15**, 136.

ROYAL SOCIETY OF CHEMISTRY

rsc.li/ees

Registered charity number: 207890

Energy & Environmental Science

ROYAL SOCIETY OF CHEMISTRY

PAPER

View Article Online
View Journal | View Issue



Cite this: *Energy Environ. Sci.*, 2022, **15**, 136

# Conversion and storage of solar energy for cooling†

Wenbin Wang, [a] Yusuf Shi,[a] Chenlin Zhang,[a] Renyuan Li, [a] Mengchun Wu, [a] Sifei Zhuo,[a] Sara Aleid[a] and Peng Wang *[ab]

Received 2nd June 2021,
Accepted 16th August 2021

DOI: 10.1039/d1ee01688a

rsc.li/ees

Global cooling demands are increasing rapidly as a result of the increasing trends of heatwaves and the increase of living standards. Meeting essential cooling demands by the impoverished is extremely challenging due to their lack of access to electricity. Herein, we report a passive design with dissolution cooling in combination with solar regeneration for the conversion and storage of solar energy for cooling without electricity consumption. As a proof of concept, cooling was achieved by dissolving a $NH_4NO_3$ salt in water and a three dimensional solar regenerator was applied to regenerate the $NH_4NO_3$ salt. The cooling power of such a system could reach up to 191 W $m^{-2}$. Importantly, the passive cooling design separates the dissolution cooling and solute regeneration physically and time-wise, allowing for energy storage and utilization even across seasons. This work shines light on the utilization of solar energy for cooling, especially for off-grid communities.

**Broader context**

Engineered cooling is essential in our daily lives as it effectively regulates the temperatures of space and substances for air conditioning, perishable substance storage, equipment temperature control, vaccine transportation and storage, *etc.* Great progress in cooling has been made in the past few decades, especially by the advancement of electricity-based vapor compression. On the other hand, the development of electricity-free cooling technologies, which are much needed in off-grid communities, remains stagnant. This work demonstrates a passive no electricity and sustainable cooling on-demand (NESCOD) system that can effectively convert and store solar energy for cooling. In the NESCOD system, the cooling is achieved by dissolving a $NH_4NO_3$ salt in water and solar energy is utilized to regenerate the salt. The cooling power of the NESCOD system reaches up to 191 W $m^{-2}$ under one-sun illumination.

## Introduction

Cooling is highly desirable in many aspects of daily human life, such as space cooling and food storage. The demand for cooling, especially space cooling, will increase rapidly due to the increasing frequency, duration and intensity of extreme heatwaves as a result of climate change in combination with steadily improved life standards.[1–4] Recent years have witnessed the great development of electricity-driven air compression-based cooling technologies. However, globally, there are over 700 million people living in impoverished regions who still do not have access to electricity and thus are unable to enjoy the modern era cooling technologies.[5] In this case, developing an inexpensive cooling technology that operates in the absence of electricity is highly desired and can significantly improve the living standards of those who are left behind by modern human development. From an economic point of view, it is preferable that the cooling power can be provided and controlled on demand in terms of intensity, locality, time and duration.

Basically, a lower space temperature can be created by heat exchange or thermal absorption. Active heat exchange, which removes heat to a high temperature region, can refrigerate at a high cooling power, but demands electricity to drive this process. In contrast, passive heat exchange can remove heat to a colder region without electricity consumption. For example, radiative sky cooling radiates heat to the cold outer space *via* the Earth's atmosphere narrow optical window which is partially transparent to mid-infrared thermal radiation (*i.e.*, 8–13 um).[6–8] As a result, it is unsurprising that the sky cooling has a low intrinsic thermodynamic cooling power limit of ~160 W $m^{-2}$.[9–11] Furthermore, it can only decrease the temperature of the area beneath the cooling material by ~10 °C.

[a] *Water Desalination and Reuse Center, Division of Biological and Environmental Science and Engineering, King Abdullah University of Science and Technology, Thuwal 23955-6900, Saudi Arabia. E-mail: peng.wang@kaust.edu.sa*
[b] *Department of Civil and Environmental Engineering, The Hong Kong Polytechnic University, Hong Kong, China*

† Electronic supplementary information (ESI) available. See DOI: 10.1039/d1ee01688a

On the other hand, thermal absorption, in which heat is transformed across different substrates (*e.g.*, from liquid bulk water or $NH_3$ to vapor sorbents), is nowadays gaining momentum.[12–14] The cooling is produced by the phase change of the liquids and the sorbents are regenerated to complete a cycle. The thermal absorption is capable of on-demand and targeted cooling with more flexibility in controlling its cooling power and thus performance than sky cooling. Nevertheless, the passive thermal absorption based-cooling system often shows a very low cooling power due to the slow diffusion of vapor in the absence of an electricity-driven artificial wind field.

Herein, we demonstrate a fully passive cooling design with chemical dissolution generating cooling while solar and low-grade environmental heat drive the chemical regeneration. The new design produces no electricity and sustainable cooling on-demand (NESCOD). The NESCOD is composed of two components: (1) chemical dissolution cooling that refrigerates by dissolving the cooling solute whose enthalpy of solution is considerably positive (*i.e.*, endothermic) and (2) solute regeneration that regenerates the cooling solute using renewable energy. Importantly, the NESCOD separates the dissolution cooling and solute regeneration physically and time-wise, allowing for energy storage and utilization even across seasons. As a proof of concept, the use of $NH_4NO_3$, whose enthalpy of saturated solution is 187.6 kJ $kg^{-1}$, as a cooling solute and three dimensional (3D)-shaped solute regenerator (3D SR) in this work led to a cooling solute regeneration rate of 4.6 kg $m^{-2}$ $h^{-1}$ under one-sun illumination, representing a cooling power of 191 W $m^{-2}$. The cooling power in $NH_4NO_3$ can be released flexibly at anytime and anywhere by dissolving $NH_4NO_3$ in water. The storage of the $NH_4NO_3$ salt is much easier than that of the vapor sorbents in thermal adsorption. Due to the fast $NH_4NO_3$ dissolution and, therefore, heat absorption rate, the temperature of the cooling solution can be decreased to $\sim -2.4$ °C in only 20 min. The NESCOD is expected to provide a new solution for low barrier-of-entry cooling that is suitable for off-grid communities.

## Results and discussion

### Design principle of the NESCOD

The process of NESCOD is shown in Fig. 1a and b. The NESCOD is composed of dissolution cooling and solute regeneration. In the dissolution cooling component, the cooling solute with a positive enthalpy of solution is dissolved in water, and this endothermic dissolution absorbs heat and thus produces a cooling effect. A maximum cooling power is achieved when the cooling solute is dissolved in water to its saturation (detailed discussion will be presented later). In the solute regeneration component, the solution is evaporated and the cooling solute is recovered. As a proof-of concept, a 3D cup-shaped solar solute regenerator (3D SR) is designed for solute regeneration.[15] The 3D SR consists of a photothermal cup made of a spectrally selective absorber (SSA). The outer surface of the 3D SR is wrapped by a very thin polyethylene (PE) film to prevent it from directly contacting with the saturated salt solution. Hydrophilic non-woven fabrics are wrapped around the outer wall of the 3D SR on the top of the PE film. Some space (1 cm height) is purposefully kept between the fabrics and cup mouth (Fig. S1, ESI†). The design of the 3D SR physically separates the light absorption area (the bottom) and the salt crystallization surface (the outer wall part), which benefits an easy and continuous collection of the crystallized cooling solute. The NESCOD design also allows for an option of evaporated water vapor collection and thus water recycling (Fig. S2, ESI†). More details about the 3D SR can be found in the ESI.†

### Cooling solute screening

The salts that can be used as cooling solutes for dissolution cooling include, but are not limited to, $NH_4NO_3$, $KNO_3$, $NaNO_3$, $NH_4Cl$, KCl, and KBr. Since the cooling solute is dissolved to its saturation for the purpose of extracting its maximum cooling power, both its water solubility and enthalpy of the saturated solution need to be considered. As shown in Table S1 (ESI†), among the salts in question, $NH_4NO_3$ shows the highest

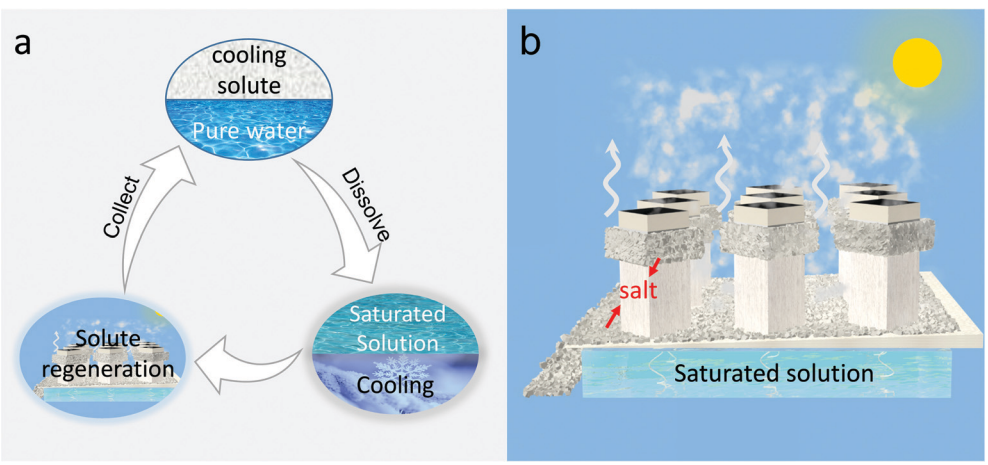


Fig. 1 Schematic illustration of the NESCOD system. (a) Cooling and regeneration cycle. (b) Solute regeneration by 3D SR.

solubility, while the $KNO_3$ has the highest enthalpy of the saturated solution.[16–21] In the NESCOD, the cooling power is stored in the cooling solute and it is regenerated by the 3D SR during solute regeneration. In this case, the cooling capacity regeneration rate ($P_r$) in the solute regeneration process can be expressed as follows:

$$P_r = \frac{1000 \times r}{3600} \times \frac{s}{100} \times \frac{1000 \times \Delta H_{sat}}{M}, \quad (1)$$

where $r$ is the evaporation rate (kg $m^{-2}$ $h^{-1}$) during the solute regeneration process by the 3D SR, $s$ is the salt solubility (g per 100 g water), $\Delta H_{sat}$ is the enthalpy of the saturated solution (kJ $mol^{-1}$) and $M$ is the molecular weight of the cooling solute (g $mol^{-1}$). It needs to be pointed out that since the saturated solubility and enthalpy of the saturated solution are both related to the temperature of the solution, these two values are obtained according to the final temperature of the solution in the dissolution cooling process.

In the dissolution cooling process, the cooling power that can be released from the cooling solute may be lower than the cooling capacity regeneration rate because part of the cooling power can be consumed by decreasing the water and cooling solute temperature. Herein, we define the cooling power ($P$) of the NESCOD as the cooling power that can be generated in a given condition and it is calculated by the following equation:

$$\begin{cases} P = P_r - P_s - P_w \\ P_w = \dfrac{1000 \times r}{3600} \times C_w \times \Delta T \\ P_s = \dfrac{1000 \times r}{3600} \times \dfrac{s}{100} \times C_s \times \Delta T \end{cases}, \quad (2)$$

where $P$, $P_r$, $P_s$ and $P_w$ are the cooling power of the NESCOD (W $m^{-2}$), the cooling capacity regeneration rate, the power consumption by water temperature reduction and the solute temperature reduction, respectively. $r$ is the evaporation rate (kg $m^{-2}$ $h^{-1}$) during the solute regeneration process by the 3D SR, $s$ is the salt solubility (g per 100 g water), $C_w$ and $C_s$ are the specific heat of water and the cooling solute, and $\Delta T$ is the temperature difference between the ambient temperature and ultimate solution temperature of the dissolution cooling system.

Since this calculation needs to be based on a given situation, we assume that the ambient temperature is 35 °C and the ultimate temperature of the solution is at a human well-being room temperature, 25 °C. Considering that the salt concentration has little effect on the evaporation rate as reported in a previous work,[22] the cooling power of different salts is calculated by assuming an evaporation rate of 1.0 kg $m^{-2}$ $h^{-1}$ during the regeneration step, as shown in Fig. 2a. The $NH_4NO_3$ shows a cooling capacity regeneration rate of 109 W $m^{-2}$ and the corresponding cooling power is calculated to be 87 W $m^{-2}$, the highest among all salts, compared with that of the other salts all $<20$ W $m^{-2}$. The enthalpy of $NH_4NO_3$ solution at different concentrations is further calculated according to eqn (S1) (ESI†). As shown in Fig. 2b, its cooling power increases along with an increasing concentration, which confirms that its saturation solution would deliver a maximum cooling power. The above results confirm the superiority of $NH_4NO_3$ among all the salts under consideration.

## Cooling power storage

The ability of the NESCOD system to store cooling power is affected by the solute regeneration rate of the regeneration system, which is related to the water evaporation rate of the 3D SR and can be calculated by multiplying the evaporation rate by the ratio of the solute to water in the saturated solution. The solar evaporation performance of the 3D SR was first evaluated by a home-made experimental setup, as illustrated in Fig. 3a. To decrease the heat loss, polystyrene (PS) foam was used for thermal insulation under the 3D SR owing to its low thermal conductivity ($\sim$0.03 W $m^{-1}$ $K^{-1}$). The liquid solution was wicked uphill into the 3D SR by a fabric strip *via* a capillary effect through a hole in the PS foam and then wetted the entire outer wall of the 3D SR.

As a control, the evaporation rates of the 3D SR with pure water as the source water under one-sun illumination and in the dark were measured to be 2.4 kg $m^{-2}$ $h^{-1}$ and 0.8 kg $m^{-2}$ $h^{-1}$,

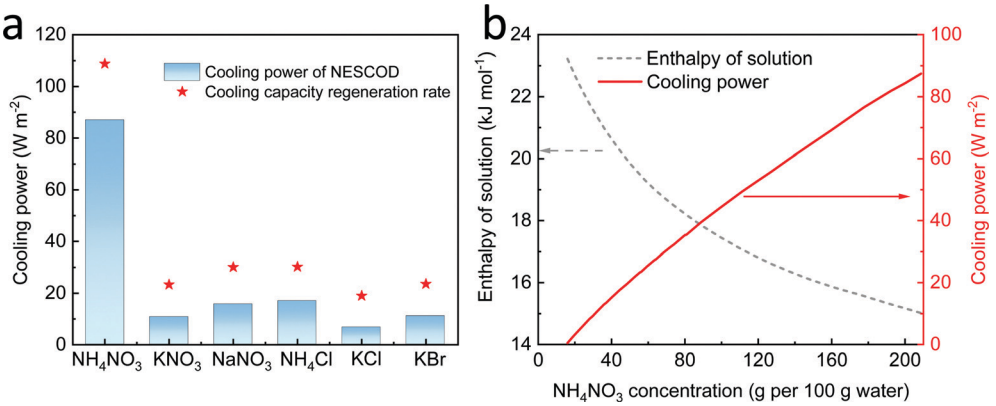


Fig. 2 Cooling power calculations. (a) Cooling power of different cooling solutes at an arbitrarily assumed evaporation rate of 1.0 kg $m^{-2}$ $h^{-1}$ during the regeneration step. (b) Enthalpy of $NH_4NO_3$ solution at different concentrations (g per 100 g water) and the corresponding cooling power at an evaporation rate of 1.0 kg $m^{-2}$ $h^{-1}$.

 

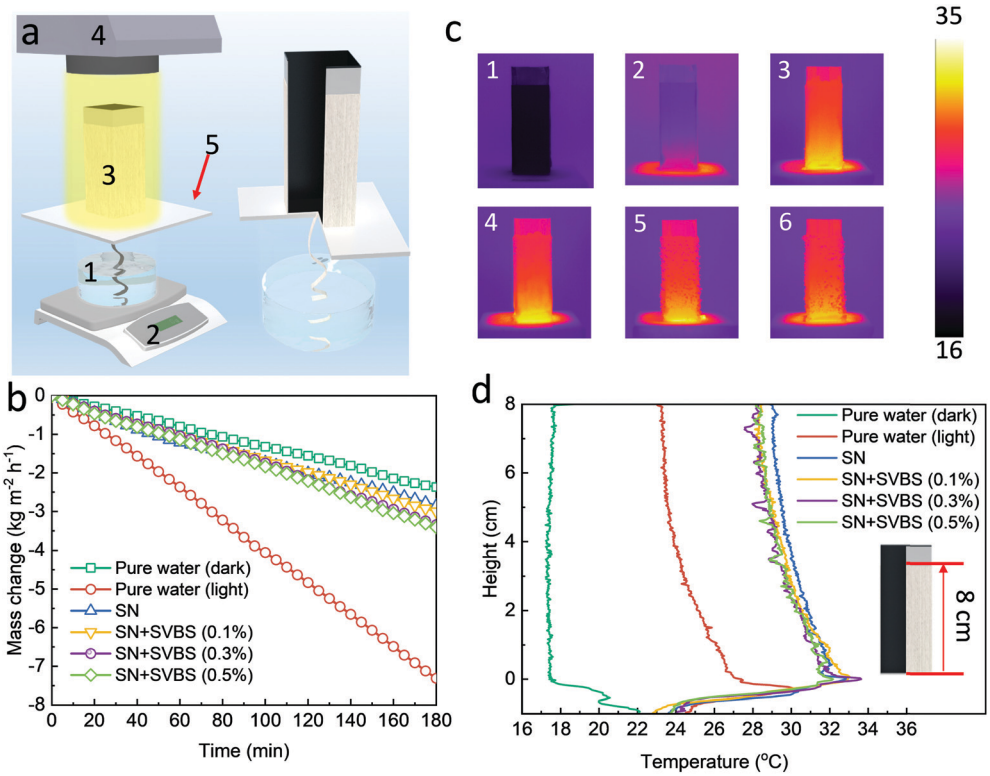


Fig. 3 Solar evaporation performance evaluation of the 3D SR. (a) Experimental setup of the solar evaporation performance measurement system. (1 source water, 2 electrical scale, 3 3D SR, 4 solar simulator, and 5 PS foam). (b) Mass change over time of the different source waters during solar evaporation. (c) IR image of the 3D SR (1) in the dark (2–6) under sunlight when the source water was (2) pure water and (3) saturated $NH_4NO_3$ (SN), and saturated $NH_4NO_3$ solution in the presence of sodium 4-vinylbenzenesulfonate (SVBS) at the concentrations of (4) 0.1%, (5) 0.3% and (6) 0.5%. (d) The surface temperature change curves of the 3D SR.

respectively (Fig. 3b), confirming that the solar evaporation performance of the 3D SR is comparable to the state-of-the-art 3D-shaped solar steam generators.[22–24] The high evaporation performance of the 3D SR should be attributed to its large water/air interface and the reabsorption of the diffuse reflectance by its wall according to the literature studies.[23] However, when the pure water was replaced with saturated $NH_4NO_3$ solution (SN), the evaporation rate was greatly decreased to 0.9 kg m$^{-2}$ h$^{-1}$, representing a $NH_4NO_3$ regeneration rate of 1.9 kg m$^{-2}$ h$^{-1}$. The decreased evaporation rate is a result of two reasons. First, the saturated solution has a decreased saturated vapor pressure. Second, the crystallized $NH_4NO_3$ salt accumulates on the outer wall of the 3D SR fabrics during crystallization and forms a compact salt crust layer (Fig. S3a, ESI†), which can block the delivery of the source water to the water/air interface. As shown in Fig. 3c (2–3) and 3d, the surface temperature of the outer wall with pure water as the source water was below the room temperature of 25 °C while it was increased to 30–33 °C when the saturated $NH_4NO_3$ solution was used as the source water. The increased outer wall temperature can partially be an indicator of an inhibited water evaporation.

During the salt crystallization, the contiguous granules can be aggregated due to the large surface tension force of the $NH_4NO_3$ solution, leading to the formation of the compact salt crust layer.[25] It has been reported that the addition of some surfactants can decrease the surface tension of the $NH_4NO_3$ solution, preventing the granule aggregation and thus leading to more loosely packed salt crystal structures.[25–27] In light of this, we added different amounts of sodium 4-vinylbenzenesulfonate (SVBS) into the saturated $NH_4NO_3$ solution with an aim to increase its evaporation rate using the 3D SR. As shown in Fig. 3b, when the concentrations of SVBS were 0.1%, 0.3% and 0.5%, the evaporation rates were increased to be 1.0, 1.1 and 1.1 kg m$^{-2}$ h$^{-1}$, representing the $NH_4NO_3$ regeneration rates of 2.1, 2.3 and 2.3 kg m$^{-2}$ h$^{-1}$, respectively. Moreover, the surface temperature of the crystallized salt in the presence of SVBS was decreased to around 29 °C (Fig. 3c and d) from 30 to 33 °C without SVBS. Meanwhile, it can be observed that some individual granules were formed on the surface of the 3D SR (Fig. S3, ESI†) and the number of these granules appeared to increase along with the SVBS concentration, indicating that the addition of SVBS decreases the aggregation of the $NH_4NO_3$ salt granules. In particular, it can be observed that there are many small peaks that represent a lower temperature on the temperature change curve in the situation when the SVBS concentrations are 0.3% and 0.5% (Fig. 3d), which can be attributed to the lower temperature of the formed granules on the surface. The formed granules add more water/air interfaces and thus enhance their evaporation rate. Therefore, with less compact crystallized salts where more

pores are present to provide pathways for water delivery, a higher evaporation rate and a lower surface temperature are then resulted. These results confirm that the addition of a small amount of SVBS into the saturated $NH_4NO_3$ solution will improve the cooling solute regeneration performance by the 3D SR.

The long-term solute regeneration performance of the 3D SR was further investigated when the saturated $NH_4NO_3$ solution with SVBS added was used as the source water. The saturated $NH_4NO_3$ solution with 0.5% SVBS that produced the highest evaporation rate (Fig. 3b) was used for the recyclability test. The SVBS content in the collected crystallized solid was measured to be $\sim$0.77 wt% (Fig. S4, ESI†), which is comparable to the weight ratio from SVBS to $NH_4NO_3$ (0.0074 : 1) in the original saturated solution. This result confirms the stability of the SVBS content in the recycled cooling solute. From this point on, the saturated $NH_4NO_3$ solution with 0.5% SVBS was used consistently to obtain the crystallized $NH_4N_3O$ salt unless otherwise specified.

In conducting salt recovery experiments, a large container was placed on the electrical scale to collect the dropped salt. As shown in Fig. S5 (ESI†), the salt crystals were loosely accumulated on the 3D SR and considerable salt crystals were collected on the PS foam after 36 hours under one-sun illumination, indicating that the salt crystals can drop off from the 3D SR by their own gravity. Compared with the pure $NH_4NO_3$ salt (Fig. S6, ESI†), the crystallized $NH_4NO_3$ salt in the presence of SVBS exhibited a larger volume at the same weight (1.0 g), manifesting that it has a higher bulk pore volume and thus surface area. Very interestingly, the evaporation rate was increased from $\sim$1.1 kg $m^{-2}$ $h^{-1}$ after the first 3 h to $\sim$2.2 kg $m^{-2}$ $h^{-1}$ at 24 h (Fig. S7, ESI†) with the corresponding solute regeneration rate being increased from 2.3 kg $m^{-2}$ $h^{-1}$ to 4.6 kg $m^{-2}$ $h^{-1}$. The increase in the evaporation rate should be attributed to the loosely accumulated salt crystals, which add more water/air interfaces for evaporation and solar energy absorption. However, our attention was attracted by the migration of the salt crystals up to the cup-mouth from 24 h to 36 h (Fig. S5, ESI†), which affected the sunlight absorption by the 3D SR. As a result, the evaporation rate decreased after 24 h and ended up with a rate of 1.8 kg $m^{-2}$ $h^{-1}$ at 36 h (Fig. S7, ESI†). We suspected that the up migration of the crystals might be due to the high surface energy of the wall material (PE film).

To confirm, we investigated the evaporation process of the saturated $NH_4NO_3$ solution with 0.5% SVBS on PE film and polytetrafluoroethylene (PTFE) film with a lower surface energy. As shown in Fig. S8a and b (ESI†), the contact angles of the saturated $NH_4NO_3$ solution with 0.5% SVBS on the PE film and PTFE film were 98.4° and 138.2°, respectively, confirming the lower surface energy of the PTFE film. Then, the solution was dropped onto the PE film and PTFE film for complete evaporation at $\sim$30 °C (Fig. S8c and d, ESI†). By the end of the evaporation, the salt crystals were dispersed on the PE film, which was far beyond the original area of the liquid drop, whereas the salt crystals on the PTFE film maintained their original shape. These results demonstrate that the utilization of the PTFE film might prevent the up migration of the salt crystals during evaporation.

To this end, a new 3D SR with the area above the fabric being wrapped by a piece of PTFE film was fabricated (Fig. 4a) and exposed under one-sun illumination for 72 h. As shown in Fig. 4b, the new 3D SR exhibited an increased evaporation rate

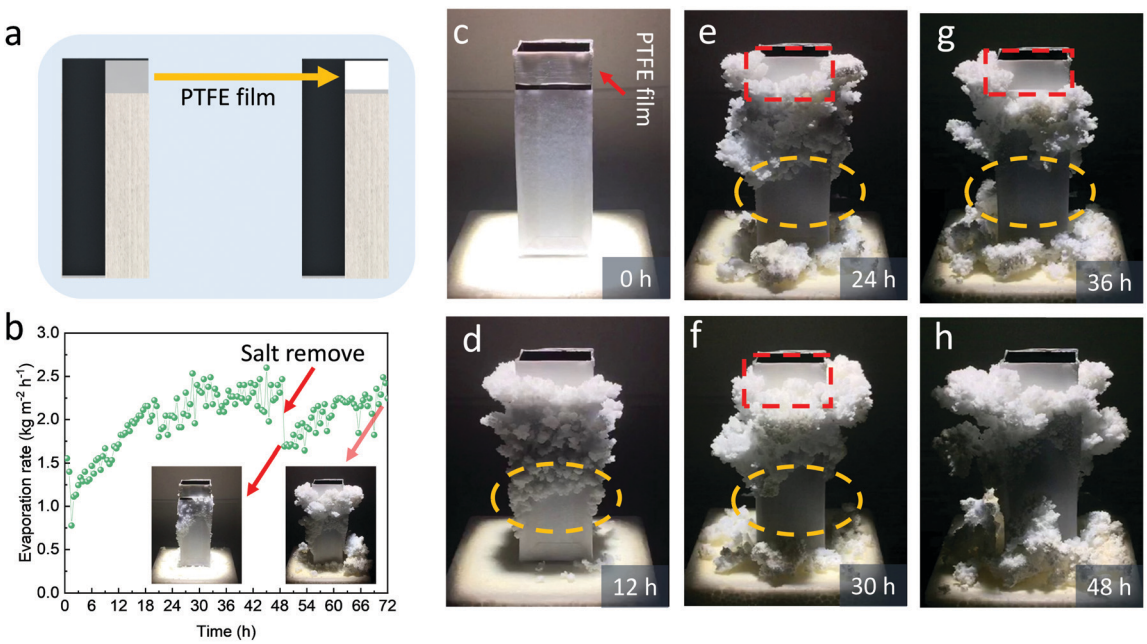


Fig. 4 Long-term crystallization performance of saturated $NH_4NO_3$ with 0.5% SVBS solution of the 3D SR with the PTFE film wrapped between the fabric and cup mouth. (a) PTFE coating on the 3D SR to prevent salt migration uphill (left: 3D SR and right: 3D SR with PTFE). (b) Evaporation rate. (c–h) Crystallization evolution.

 

from ~1.1 kg $m^{-2}$ $h^{-1}$ to ~2.2 kg $m^{-2}$ $h^{-1}$ at 24 h, and the evaporation rate kept stable thereafter in the following 24 h. Its evaporation performance within the first 24 hours was similar to the 3D SR without the PTFE film, indicating that the presence of the PTFE film has little effect on the evaporation performance of the 3D SR. The images of the salt crystals on the new 3D SR are shown in Fig. 4b–h. As seen, the loosely packed salt crystals could clear themselves off the 3D SR as time went on (the yellow circle in Fig. 4d–g). Nevertheless, some salt crystals still migrated upwards beyond the fabric and partially covered the PTFE film. Fortunately, these salt crystals dropped off the PTFE film automatically (the red mark in Fig. 4e–g) at a certain time. As a result, the cup mouth was never covered by the salt crystals even after the 3D SR was illuminated for 48 h (relative to the 36 h illumination of the 3D SR without the PTFE film) and consequently, no apparent evaporation rate decline was observed after 24 h (Fig. 4b).

During crystallization, the drop of the crystallized salt from the 3D SR decreases the water/air interface and the light-absorbing area, leading to a transiently decreased evaporation rate. However, the evaporation continuously produces salt crystals on the 3D SR. As a result, the 3D SR exhibited a fluctuated change in the evaporation rate. To further demonstrate that the increased evaporation rate of the 3D SR is caused by the enlarged area of the accumulated salt crystals, we removed the part of the crystallized salt attached on the fabrics at 48 h (insert of Fig. 4b) and the device exhibited a steep decrease in the evaporation rate thereafter, confirming that the enhanced evaporation performance is attributed to the loosely accumulated $NH_4NO_3$ salt. In the following 24 h, the evaporation rate was gradually recovered to ~2.2 kg $m^{-2}$ $h^{-1}$. The total collected $NH_4NO_3$ salt was measured to be ~251.1 g and the evaporated water in this process was 131.4 g. The amount of the collected salt was slightly lower than the calculated one based on a full salt recovery (268.7 g) presumably because some salt was attached on and not removed from the 3D SR.

In the NESCOD system, $NH_4NO_3$ needs to be crystallized and dissolved multiple times. To simulate this scenario, 5 crystallization cycles were conducted. In each cycle, the crystallized salt was redissolved in water to saturation to generate cooling followed by solute regeneration during which the 3D SR was exposed under one-sun illumination for 8 h, followed by keeping in the dark overnight. Since the weight ratio of SVBS-to-$NH_4NO_3$ in solution and crystallized salt was stable, there was no further addition of SVBS in the entire process. As shown in Fig. 5a, the 3D SR exhibited an increased evaporation rate from 1.4 to 1.9 kg $m^{-2}$ $h^{-1}$ in the first 2 cycles and kept stable at ~2.2 kg $m^{-2}$ $h^{-1}$ in the following 3 cycles. In other words, the device reached a stable evaporation rate after the first 2 cycles and it can be calculated that the accumulated illumination time is only 16 h, which is shorter as compared to the continuous evaporation test (Fig. 4b). This can be attributed to the continuous evaporation during the night because the device was kept in the dark after illumination. Under the conditions that the evaporation rate and solute regeneration rate of the 3D SR are ~2.2 kg $m^{-2}$ $h^{-1}$ and ~4.6 kg $m^{-2}$ $h^{-1}$, respectively, the cooling capacity regeneration rate was calculated to be 239 W $m^{-2}$, representing a cooling power of 191 W $m^{-2}$ (Fig. 5b). It was emphasized that this calculation was based on the assumption that the ultimate solution temperature was 25 °C and the ambient temperature was 35 °C. At a lower solution temperature, $NH_4NO_3$ solubility is reduced while the corresponding enthalpy of the saturated solution is increased (Fig. S9a, ESI†). According to equations 1 and 2, it can be calculated that the cooling power is reduced at a lower temperature, *e.g.*, from 191 W $m^{-2}$ at 25 °C to 57 W $m^{-2}$ at 0 °C (Fig. S9b, ESI†) when the evaporation rate is 2.2 kg $m^{-2}$ $h^{-1}$. In some practical situations, the temperature of the system needs to be maintained at 5–15 °C and the corresponding cooling power is in the range of 81–134 W $m^{-2}$. Efforts were also made to condense the vapor to produce liquid water. The ion concentration and total organic carbon of the collected liquid water were measured to be less than 1 ppm, demonstrating that no $NH_4NO_3$ and SVBS were evaporated (Fig. 5c). The above results show that the NESCOD has a high specific cooling power, a good stability and recyclability.

### Cooling performance evaluation

The cooling performance of the pure $NH_4NO_3$ salt and the crystallized $NH_4NO_3$ salt along with the added SVBS was further

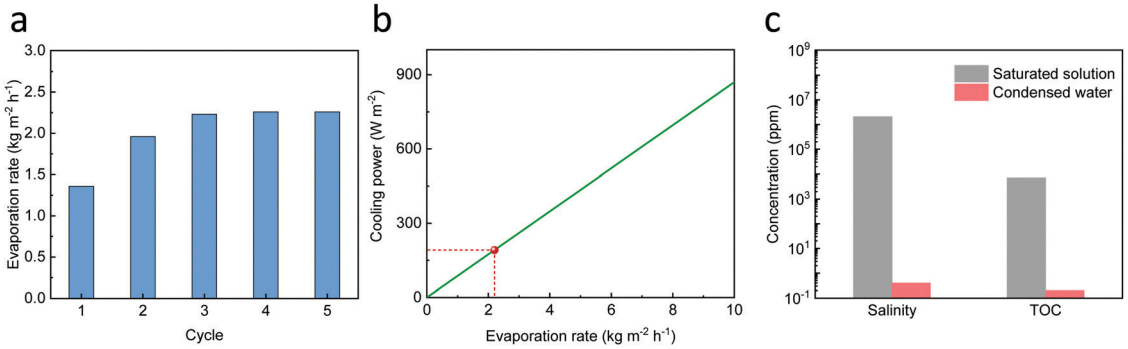


Fig. 5 Reusability evaluation. (a) The evaporation performance of the 3D SR in different cycles when the crystallized $NH_4NO_3$ salt with SVBS was redissolved in water and used as the source water. (b) Salinity and total organic carbon (TOC) of the condensed water. (c) The cooling power of the NESCOD system as a function of the evaporation rate when $NH_4NO_3$ was used as the cooling solute.

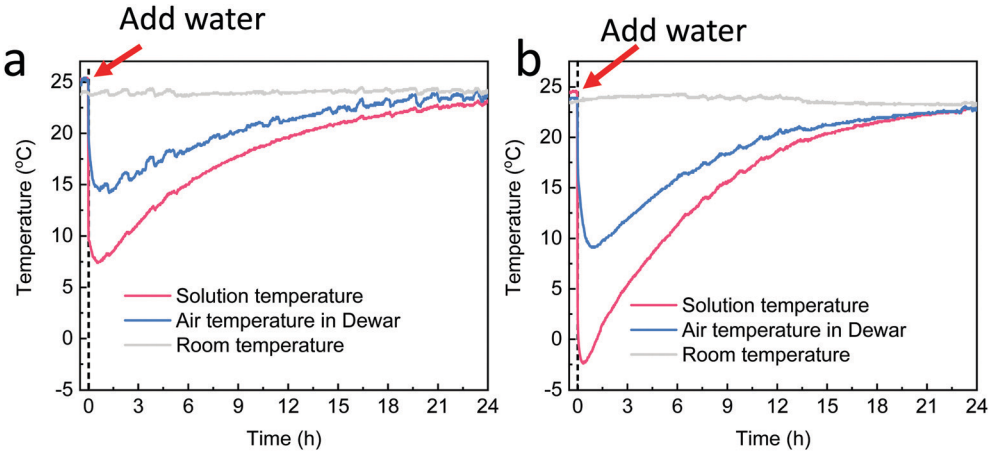


Fig. 6 Cooling performance comparison between the $NH_4NO_3$ salt and $NH_4NO_3$/SVBS salt. The temperature change of the cooling system caused by dissolving the (a) pure $NH_4NO_3$ salt and (b) $NH_4NO_3$/SVBS salt.

investigated. In performing the experiment, excess salt was first added to the Dewar to ensure the formation of a saturated solution, followed by the addition of water. The temperature of the solution, air temperature of the head space in the Dewar and room temperature were monitored by thermal couples (Fig. S10a, ESI†). After water was added in pure $NH_4NO_3$ salt, the temperature of the solution was decreased by ~16.6 °C in 27 min, from a room temperature of ~24 °C to around ~7.4 °C (Fig. 6a). Due to the natural heat transfer, the air temperature in the Dewar was decreased to 14.2 °C in 76 min, having a temperature disparity of ~9.8 °C. Moreover, the temperature of the solution and air in the Dewar was kept below room temperature for over 20 hours. The long cooling duration can be attributed to the continuous dissolution of the $NH_4NO_3$ salt and good thermal insulation of the Dewar (for more details, see Note S.1, ESI†).

When the crystallized $NH_4NO_3$ salt was utilized as the cooling solute, the solution in the Dewar decreased to a lower temperature at ~−2.4 °C in only 20 min, having a higher maximum temperature disparity of 26.4 °C. Accordingly, the air temperature in the Dewar was decreased by 14.9 °C and reached a minimum temperature of 9.1 °C in 51 min. As compared with the pure $NH_4NO_3$ salt, the crystallized $NH_4NO_3$ salt had a lower minimum temperature due to its higher surface area and consequently a higher dissolution rate (for more details, see Note S.1, ESI†). Moreover, it took over 20 h for the system to reach room temperature. To confirm the continuous dissolution of the $NH_4NO_3$ salt during this period, the same amount of cold water that was kept in a refrigerator (4 °C) overnight was dumped into the Dewar and the temperature change is shown in Fig. S10 (ESI†). The bottom temperature of the Dewar was only decreased to ~8.8 °C after the addition of cold water and was increased to ~23.2 °C in 12 h. The temperature increase (from ~9 °C) of the $NH_4NO_3$ solution (with SVBS) is also depicted in Fig. S10b (ESI†) for comparison (dash line). As compared to the cold water, the $NH_4NO_3$ solution exhibits a slower temperature increase by the end of 12 h; it only increased to 21.1 °C. This result confirms that the slower temperature elevation of the $NH_4NO_3$ solution should be attributed to the continuous dissolution of the undissolved salt.

Furthermore, we designed a cooling system for food storage with some simple and easily available materials. The cooling system was made of a metal cup for food storage and a polystyrene (PS) foam box for heat insulation (Fig. S11a, ESI†). The side area of the PS foam box was filled with the $NH_4NO_3$ salt. In the test, water was added in two steps. First, half of the water was dumped into the PS foam box at once and then the other half was added at a flow rate of 1 ml $min^{-1}$ within a duration of 180 min by a home-made gravity-driven system, which was composed of a bottle and an outlet (Fig. S11b, ESI†). During the operation, the bottle was placed to be higher than the box and sealed by a lid. When the water flows out, the height of the water level was decreased, and the air flows into the bottle *via* the air filter on the outlet. This design allows the system to keep a stable pressure, leading to a stable flow rate. The flow rate can be modulated by a clip on the water pipe. A similar structure and the stable flow rate have been demonstrated in our previous report.[28] As shown in Fig. S11c (ESI†), the temperature of the cup was reduced to ~6.2 °C in 26 min after the dumping of the first half of the water and then decreased slowly to ~3.6 °C in 220 min before slowly increasing to room temperature thereafter. The temperature of the cup was maintained below 10 °C for over 8 h and 15 °C for over 15 h, indicating a good food storage ability. Overall, these results demonstrated that the NESCOD is capable of refrigerating rapidly and this process is controllable to meet various demands.

## Outlook

In the NESCOD, each cycle consists of 2 steps: (1) the dissolution of the cooling solute (*e.g.*, $NH_4NO_3$ salt) to absorb heat and decrease the surrounding temperature, leading to a cooling effect and (2) cooling solute crystallization and regeneration. The NESCOD system is fully passive as no electricity, no high-pressure compression, and mechanically moving parts are involved during its operation. More importantly, solar energy,

 

which is clean, green, widely available, and renewable, is utilized as the only energy source, which is significant in alleviating our reliance on electricity. All these features make it a promising passive cooling technology with a negligible environmental impact.

In theory, the cooling power in NESCOD is converted from solar energy and is stored in $NH_4NO_3$, which can be released on demand. The stored cooling energy density of $NH_4NO_3$ is calculated to be 189 kJ $kg^{-2}$ (25 °C), which is comparable with the energy density of phase change materials that are generally used for heat storage.[29] Since $NH_4NO_3$ is stable under normal environmental conditions and is also widely used in agriculture as a high-nitrogen fertilizer,[30] the long-term storage and preservation of $NH_4NO_3$ are not challenging. This allows for solar energy utilization to regenerate the cooling solute in winter and then the cooling application in summer, leading to sufficient and cross-seasonal solar energy utilization.

The cooling power of the NESCOD can be significantly affected by the properties of the cooling solute (*i.e.*, solubility and enthalpy of the saturated solution) and solar regeneration (*i.e.*, evaporation rate and salt crystallization performance). Therefore, the NESCOD has a huge potential to realize a higher cooling power. Specifically, the cooling power can be enhanced by adopting some other cooling solute substances that have a higher solubility and/or enthalpy of the saturated solution. The cooling solute can be a pure substance or a mixture. On the other hand, the cooling power can be promoted by increasing the energy efficiency of the solute regeneration device *via* various means.[31–36] These promises call for further research efforts.

The NESCOD system can be tailored for various application scenarios. In particular, it is well-suited to providing cooling power for off-grid communities that have limited access to electricity. The NESCOD system can be an essential home appliance in these places to meet different purposes. For example, it can be used to decrease the temperature of the bed on demand in summer when sleeping. In many rural regions of China, kangs are widely used as a bed for sleeping in winter as they use the hot exhaust from the burning of firewood to create a warm bed. Similarly, a bed at a human well-being temperature can be designed for comfortable sleep in the summer by utilizing the cooling power of dissolving the cooling solute and this consumes less energy as compared to cooling the entire room. The NESCOD can also be used for building cooling. The solute regeneration device can be installed on the building roof, while the cooling system can be placed in the room and used when needed.

## Conclusion

Overall, we successfully develop a passive no electricity and sustainable cooling on-demand (NESCOD) system that can convert and store solar energy for cooling. The system is composed of two components: chemical dissolution cooling and solar solute regeneration, which separates the dissolution cooling and solute regeneration physically and time-wise, allowing for energy storage and utilization even across seasons. Notably, the simple dissolution process that absorbs heat allows it to meet various cooling demands. The NESCOD represents a fully renewable energy-driven, green cooling technology without electricity consumption, which is urgently desired in our fight against global warming. The development of the NESCOD opens a new era to provide a low barrier-of-entry cooling power especially suitable for off-grid communities. It fills the existing gaps in cooling technologies and has the potential to make a meaningful contribution to achieving universal SDGs by 2030.

## Experimental procedures

### Materials

The non-woven fabrics used as the strips were provided by Kimberly-Clark. Ammonium nitrate and sodium 4-vinylbenzenesulfonate (SVBS) were purchased from Sigma-Aldrich. Spectra selective absorber ETA@Al was purchased from Alanod Solar. The polyethylene (PE) film was purchased from Zhichuang (China).

### Fabrication of the 3D SR

The spectrally selective absorber (SSA) sheet was made into a cup shape as illustrated in Fig. 1c, with a plastic cup being used as a mold and the junction was sealed by aluminum tape. The polyethylene (PE) film was stuck to the 3D SR, followed by the attachment of the fabrics.

### Water evaporation and crystallization measurement

The 3D SR was placed on the top of the square of the polystyrene (PS) foam with a length of 9 cm and a thickness of 1 cm. The PS foam was placed on the top of the source water container. The source water was wicked from the bulk water to the fabrics of the 3D SR *via* a fabric belt through a hole in the center of the PS foam. The mass change of the system was monitored by an electrical scale and recorded by a computer. Simulated sunlight was provided using a solar simulator (Newport 94043A) with a standard AM 1.5 G spectrum optical filter. During the long-term experiment, a second-container was placed under the source water container to collect the dropped $NH_4NO_3$ salt. All the measurements were conducted at a room temperature of ~24 °C with a humidity of ~55%.

### Cooling performance measurement

320 g of $NH_4NO_3$ salt was placed in a round Dewar with a diameter of 12 cm and a height of 25 cm. A thermal couple was placed in the bottom of the Dewar, and the other thermal couple was placed 8 cm above the bottom of the Dewar to monitor the temperature of ambient air in the heat space in the Dewar. 150 g of pure water was added to the Dewar and thereafter the Dewar was covered by PS foam with a thickness of 4 cm.

In the home-made food storage system, the metal cup was placed in the center of the polystyrene (PS) foam box. The side area was filled with the $NH_4NO_3$ salt. To make full use of the space, the salt was ground into powders. A thermal couple was stuck to the bottom of the cup to monitor its temperature change and then the cup was covered by a heavy lid. The gravity-driven flow system was composed of a bottle and an outlet (Fig. S11b, ESI†). The bottle was placed to be higher than the box and covered by a lid. The flow rate was modulated to be 1 ml $min^{-1}$ (calibrated by an electrical scale) by a clip on the water pipe. The test started when 200 ml of pure water was dumped into the box. The water pipe was inserted into the box and then the PS foam box was covered by a PS foam lid.

### Characterization

UV-vis-NIR diffuse reflectance spectra were recorded using an Aglient Cary 5000 spectrometer. The IR image was taken using a FLIR A655 infrared camera. The weight change as a function of temperature was measured using a TG 209 F1thermogravimetric analysis (TGA) device.

## Author contributions

W. W., Y. S. and P. W. designed the experiments. W. W. conducted the experiments. W. W. and C. Z. analyzed the data. P. W. and W. W. wrote the paper. All the authors commented on the manuscript drafts.

## Conflicts of interest

The authors declare no competing interests.

## Acknowledgements

The authors are grateful to the KAUST for very generous financial support.

## References

1 T. Li, Y. Zhai, S. He, W. Gan, Z. Wei, M. Heidarinejad, D. Dalgo, R. Mi, X. Zhao, J. Song, J. Dai, C. Chen, A. Aili, A. Vellore, A. Martini, R. Yang, J. Srebric, X. Yin and L. Hu, A radiative cooling structural material, *Science*, 2019, **364**, 760–763.

2 H. S. Laine, J. Salpakari, E. E. Looney, H. Savin, I. M. Peters and T. Buonassisi, Meeting global cooling demand with photovoltaics during the 21st century, *Energy Environ. Sci.*, 2019, **12**, 2706–2716.

3 R. Khosla, N. D. Miranda, P. A. Trotter, A. Mazzone, R. Renaldi, C. McElroy, F. Cohen, A. Jani, R. Perera-Salazar and M. McCulloch, Cooling for sustainable development, *Nat. Sustainability*, 2021, **4**, 201–208.

4 S. Perkins-Kirkpatrick and S. Lewis, Increasing trends in regional heatwaves, *Nat. Commun.*, 2020, **11**, 1–8.

5 J. Ayaburi, M. Bazilian, J. Kincer and T. Moss, Measuring ''Reasonably Reliable'' access to electricity services, *Electr. J.*, 2020, **33**, 106828.

6 A. P. Raman, M. A. Anoma, L. Zhu, E. Rephaeli and S. Fan, Passive radiative cooling below ambient air temperature under direct sunlight, *Nature*, 2014, **515**, 540–544.

7 M. M. Hossain and M. Gu, Radiative cooling: principles, progress, and potentials, *Adv. Sci.*, 2016, **3**, 1500360.

8 Q. Xia, C. Chen, T. Li, S. He, J. Gao, X. Wang and L. Hu, Solar-assisted fabrication of large-scale, patternable transparent wood, *Sci. Adv.*, 2021, **7**, eabd7342.

9 M. Alberghini, M. Morciano, M. Fasano, F. Bertiglia, V. Fernicola, P. Asinari and E. Chiavazzo, Multistage and passive cooling process driven by salinity difference, *Sci. Adv.*, 2020, **6**, eaax5015.

10 E. A. Goldstein, A. P. Raman and S. H. Fan, Sub-ambient non-evaporative fluid cooling with the sky, *Nat. Energy*, 2017, **2**, 1–7.

11 S. Buddhiraju, P. Santhanam and S. Fan, Thermodynamic limits of energy harvesting from outgoing thermal radiation, *Proc. Natl. Acad. Sci. U. S. A.*, 2018, **115**, E3609–E3615.

12 M. Liakh and O. Rabinovich, Heat and Mass Transfer in Adsorption-chemical Cooling with Phase Transitions in a Sorbent, *Heat Transfer Eng.*, 2018, **39**, 1308–1317.

13 R. Sharma and E. A. Kumar, Performance evaluation of simple and heat recovery adsorption cooling system using measured NH3 sorption characteristics of halide salts, *Appl. Therm. Eng.*, 2017, **119**, 459–471.

14 A. A. Askalany, A. Freni and G. Santori, Supported ionic liquid water sorbent for high throughput desalination and drying, *Desalination*, 2019, **452**, 258–264.

15 C. Zhang, Y. Shi, L. Shi, H. Li, R. Li, S. Hong, S. Zhuo, T. Zhang and P. Wang, Designing a next generation solar crystallizer for real seawater brine treatment with zero liquid discharge, *Nat. Commun.*, 2021, **12**, 1–10.

16 A. W. Stelson and J. H. Seinfeld, Relative-Humidity and Temperature-Dependence of the Ammonium-Nitrate Dissociation-Constant, *Atmos. Environ.*, 1982, **16**, 983–992.

17 A. Sanahuja and J. L. Gomezestevez, A New Evaluation of the Relative Apparent Molar Enthalpies of KCl in Water at 298.15 K, *Thermochim. Acta*, 1987, **117**, 105–114.

18 A. Apelblat, The Vapor-Pressures of Saturated Aqueous-Solutions of Potassium-Bromide, Ammonium-Sulfate, Copper(II) Sulfate, Iron(II) Sulfate, and Manganese(II) Dichloride, at Temperatures from 283 K to 308 K, *J. Chem. Thermodyn.*, 1993, **25**, 1513–1520.

19 A. Apelblat and E. Korin, The vapour pressures of saturated aqueous solutions of sodium chloride, sodium bromide, sodium nitrate, sodium nitrite, potassium iodate, and rubidium chloride at temperatures from 227 K to 323 K, *J. Chem. Thermodyn.*, 1998, **30**, 59–71.

20 A. Apelblat and E. Korin, Vapour pressures of saturated aqueous solutions of ammonium iodide, potassium iodide, potassium nitrate, strontium chloride, lithium sulphate, sodium thiosulphate, magnesium nitrate, and uranyl nitrate from T = (278 to 323) K, *J. Chem. Thermodyn.*, 1998, **30**, 459–471.

 

21 C. Vanderzee, D. H. Waugh and N. C. Haas, Enthalpies of dilution and relative apparent molar enthalpies of aqueous ammonium nitrate. The case of a weakly hydrolysed (dissociated) salt, *J. Chem. Thermodyn.*, 1980, **12**, 21–25.

22 Y. Shi, C. Zhang, R. Li, S. Zhuo, Y. Jin, L. Shi, S. Hong, J. Chang, C. Ong and P. Wang, Solar Evaporator with Controlled Salt Precipitation for Zero Liquid Discharge Desalination, *Environ. Sci. Technol.*, 2018, **52**, 11822–11830.

23 Y. Shi, R. Y. Li, Y. Jin, S. F. Zhuo, L. Shi, J. Chang, S. Hong, K. C. Ng and P. Wang, A 3D Photothermal Structure toward Improved Energy Efficiency in Solar Steam Generation, *Joule*, 2018, **2**, 1171–1186.

24 J. H. Zhou, Y. F. Gu, P. F. Liu, P. F. Wang, L. Miao, J. Liu, A. Y. Wei, X. J. Mu, J. L. Li and J. Zhu, Development and Evolution of the System Structure for Highly Efficient Solar Steam Generation from Zero to Three Dimensions, *Adv. Funct. Mater.*, 2019, **29**, 1903255.

25 J. Whetstone, Solution to the Caking Problem of Ammonium Nitrate and Ammonium Nitrate Explosives, *Ind. Eng. Chem.*, 1952, **44**, 2663–2667.

26 B. I. Elzaki and Y. J. Zhang, Anti-hygroscopic surface modification of ammonium nitrate (NH4NO3) coated by surfactants, *Arabian J. Chem.*, 2020, **13**, 3460–3473.

27 A. Tyc, J. Hoffmann and A. Biskupski, Anti-caking agents for ammonium nitrate fertilizers. Part 1. Caking phenomenon, *Przem. Chem.*, 2019, **98**, 771–776.

28 W. Wang, A. Sara, Y. Shi, C. Zhang, R. Li, M. Wu, S. Zhuo and P. Wang, Integrated Solar-driven PV Cooling and Seawater Desalination with Zero Liquid Discharge, *Joule*, 2021, DOI: 10.1016/j.joule.2021.05.010.

29 F. Kuznik and J. Virgone, Experimental assessment of a phase change material for wall building use, *Appl. Energy*, 2009, **86**, 2038–2046.

30 K. A. Mcvay, D. E. Radcliffe and W. L. Hargrove, Winter Legume Effects on Soil Properties and Nitrogen-Fertilizer Requirements, *Soil Sci. Soc. Am. J.*, 1989, **53**, 1856–1862.

31 X. Y. Zhou, F. Zhao, Y. H. Guo, Y. Zhang and G. H. Yu, A hydrogel-based antifouling solar evaporator for highly efficient water desalination, *Energy Environ. Sci.*, 2018, **11**, 1985–1992.

32 X. Qian, Y. Zhao, Y. Alsaid, X. Wang, M. Hua, T. Galy, H. Gopalakrishna, Y. Yang, J. Cui and N. Liu, Artificial phototropism for omnidirectional tracking and harvesting of light, *Nat. Nanotechnol.*, 2019, **14**, 1048–1055.

33 J. L. Li, X. Y. Wang, Z. H. Lin, N. Xu, X. Q. Li, J. Liang, W. Zhao, R. X. Lin, B. Zhu, G. L. Liu, L. Zhou, S. N. Zhu and J. Zhu, Over 10 kg $m^{-2}$ $h^{-1}$ Evaporation Rate Enabled by a 3D Interconnected Porous Carbon Foam, *Joule*, 2020, **4**, 928–937.

34 Y. Xia, Y. Li, S. Yuan, Y. Kang, M. P. Jian, Q. F. Hou, L. Gao, H. T. Wang and X. W. Zhang, A self-rotating solar evaporator for continuous and efficient desalination of hypersaline brine, *J. Mater. Chem. A*, 2020, **8**, 16212–16217.

35 Z. Y. Xu, L. N. Zhang, L. Zhao, B. J. Li, B. Bhatia, C. X. Wang, K. L. Wilke, Y. Song, O. Labban, J. H. Lienhard, R. Z. Wang and E. N. Wang, Ultrahigh-efficiency desalination via a thermally-localized multistage solar still, *Energy Environ. Sci.*, 2020, **13**, 830–839.

36 L. N. Zhang, Z. Y. Xu, L. Zhao, B. Bhatia, Y. Zhong, S. Gong and E. N. Wang, Passive, high-efficiency thermally-localized solar desalination, *Energy Environ. Sci.*, 2021, **14**, 1771–1793.